Chapter 2

Bat algorithm optimized extreme learning machine: A new modeling strategy for predicting river water turbidity at the United States

Salim Heddam

Laboratory of Research in Biodiversity Interaction Ecosystem and Biotechnology, Hydraulics Division, Agronomy Department, Faculty of Science, Skikda, Algeria

1. Introduction

Water turbidity (TU) among other water variables has been used for a long time as an indicator of water quality in rivers, streams, and lakes freshwater ecosystems (Zolfaghari et al., 2020), and also for monitoring water contamination and guiding pollution control (Gu et al., 2020). The concentration of TU in water comes from the high concentration of the suspended solids caused by watershed runoff (Park et al., 2017), and it is often used as an indicator of the intensity of light scattering (Gelda et al., 2009; Gelda and Effler, 2007). The water clarity and transparency are measured and evaluated using the turbidity which is related to the scattering of light (Al-Yaseri et al., 2013). A high concentration of TU in freshwater can cause serious problems and lead to a deterioration of the water quality that can cause serious health problems, affecting the metabolic activity and leading to a significant increase in the net sedimentation rate (Gelda et al., 2013). In a study conducted in the Niulan River, China, it was demonstrated that high levels of turbidity were originated from three sources namely; interflows and underflows caused the sudden spikes, strong mixing caused by the floods, and the very low settling velocity of the very fine incoming sediments (Zhang and Wu, 2020). In addition, it was reported that the higher the TU concentration in water, the higher the esthetic impairments manifested (Gelda and Effler, 2007). River TU is highly correlated to river discharge (Q) and the relation between TU and Q is a complex and dynamic process (Mather and Johnson, 2014). Water TU can be measured directly using in-situ sensors and calculated using various indirect methods based on the application of different kinds of models. Over the years, several models have been developed and proposed for predicting TU and mainly based on the artificial intelligence paradigms or remote sensing data.

Rajaee and Jafari (2018) applied several machine learning for predicting daily river TU in the Blue River at Kenneth Road, Overland Park, Kansas, United States. The authors used the standard artificial neural network (ANN), gene expression programming (GEP), and the decision tree (DP) approaches. In addition, the proposed models were applied combined with the discrete wavelet transforms (DWT) for improving the model's accuracy. Based on the correlation coefficients, the explanatory variables were composed of turbidity and river discharge (Q) measured at several previous lag times. From the obtained results, the authors demonstrated that the best accuracy was achieved using the wavelet-gene expression programming (WGEP), compared to the wavelet-ANN (WANN) and wavelet-decision tree (WDT). In another study, Liu and Wang (2019) compared the multiple linear regression (MLR) and the GEP models in predicting water turbidity measured at two reservoirs located in Taiwan: the Tseng-Wen and Nan-Hwa reservoirs. The authors have developed the predictive models based on the satellite imagery obtained from the Landsat 8 satellite, and in total four inputs were selected namely, the spectral wavelength band 2 (450–510 nm, blue), band 3 (530–590 nm, green), band 4 (640–670 nm, red), and band 5 (850–880 nm). From the obtained results, the GEP model worked best compared to the MLR model. Zounemat-Kermani et al. (2020) used several machines in predicting river TU in Brandywine Creek, Pennsylvania,

Handbook of HydroInformatics. https://doi.org/10.1016/B978-0-12-821285-1.00005-1

United States, namely the online sequential extreme learning machine (OS-ELM), the ANN, the classification and regression tree (CART), the group method of data handling (GMDH), and the response surface method (RSM) models. The proposed machine learning models were developed using several predictors, i.e., Q, precipitation (P), water pH, suspended sediment (SS), dissolved oxygen (DO), and water temperature (TE). From the obtained results, they reported that the best accuracy was obtained using the OSELM model, while the CART was the worst model. Gu et al. (2020) proposed a new model for river TU retrieval using the random forest regression model (RF). The authors selected 13 bands from the hyperspectral remote sensing data obtained by the Google earth engine (GEE) and the model was called RFE-GEE. To demonstrate the superiority of the proposed RFE-GEE model, they compared its accuracy with those of RF, broad learning system (BLS), bidirectional ELM (BELM), support vector regression (SVR), deep belief network, extreme learning machine (ELM), and stacked selective ensemble-backed predictor (SSEP) models. From the obtained results, they reported that the high accuracy was obtained using the developed RFE-GEE which ensured a 15.4% gain taking into account the mean squared error (MSE). Allam et al. (2020) proposed the use of the Landsat 8 surface reflectance (L8SR) for predicting TU in the Ramganga River, India. The proposed algorithm achieved a good correlation between in situ measured and calculated river TU with $R^2 \approx 0.760$.

Najah et al. (2013) compared two artificial neural network models namely the MLPNN and the radial basis function neural networks (RBFNN) for predicting river TU measured in the Johor River Basin located in Johor state, Malaysia. The two models were developed and compared using only the total dissolved solids (TDS), and the results showed that the RBFNN ($R^2 \approx 0.80$) was more accurate compared to the MLPNN ($R^2 \approx 0.64$). Mather and Johnson (2016) combined three input variables namely river Q, P and air temperature (TE) for forecasting daily River TU 3 days in advance. The empirical even model was developed using data from two USGS sites and acceptable accuracy was obtained. Tsai and Yen (2017) used the group method of data handling algorithm (GMDH) for forecasting river TU measured at the Chiahsien Weir and its upper stream in Taiwan. By combining the Q, P, and TU measured at the previous lag, they demonstrated that GMDH ($R \approx 0.975$) was more accurate than the stepwise regressive (SGMDH) ($R \approx 0.965$) and achieved high accuracy. In a recently published paper, Teixeira et al. (2020) compared MLPNN and the fuzzy inference system (FIS) in predicting river TU using the Q and the area of the watersheds (A). According to the obtained results, the FIS model was more accurate with Nash-Sutcliffe efficiency (NSE) of 0.860 for the validation dataset. In the same context, Iglesias et al. (2014) has proposed a new modeling strategy for modeling river TU in the Nalón river basin, Northern Spain. The proposed approach used the so-called synergistic variables which were obtained by the multiplication two well-known variables: conductivity × ammonium, conductivity × pH, conductivity × dissolved oxygen, and so on. It was demonstrated that the new synergistic variables contribute significantly to the improvement of the model's performances.

According to the literature review discussed earlier, it is clear that several attempts have been done for providing general frameworks for the river water TU modeling, and models based on machine learning were the most reported tools. While it was shown that river TU can be predicted very well using a combination of several water variables, we believe that the introduction of new working methods based on the use of fewer predictor will be a very promising area of research and the development of new modeling strategy can help in improving our understanding of the river TU modeling. In addition, the use of hybrid models based on the combination of standalone machine learning and several metaheuristics algorithms can help in improving the models performances. Consequently, the objective of this study is to introduce a new kind of machine learning models called bat algorithm optimized extreme learning machine (Bat-ELM) for predicting daily river turbidity using only river discharge. The Bat-ELM was compared to the feedforward artificial neural network (FFNN), and the dynamic evolving neural-fuzzy inference system (DENFIS) models.

2. Study area and data

The study area for this investigation was composed of four USGS stations, two of them located in the Sprague River, Oregon, United States, and the two other stations in the Clackamas County, Oregon, United States. The selected stations were: (i) USGS 11497500 at Sprague River near Beatty, Klamath Basin, Oregon, United States (Latitude 42°26′51.9″, Longitude 121°14′18.7″ NAD83), (ii) USGS 11501000 at Sprague River near Chiloquin, Klamath Basin, Oregon, United States (Latitude 42°35′03.5″, Longitude 121°50′54.0″ NAD83), (iii) USGS 14210000 at Clackamas River at Estacada, Oregon, United States (Latitude 45°18′00″, Longitude 122°21′10″ NAD27), and (iv) USGS 14211010 at Clackamas River near Oregon City, Oregon, United States (Latitude 45°22′46″, Longitude 122°34′34″ NAD27). The location of the study

FIG. 1 Location map showing the four USGS stations selected for modeling river turbidity.

area shows the four USGS station in Fig. 1. The data from these four selected stations were used to build machine learning models for estimating river turbidity measured at a daily time scale, as a function of the river discharge. The length of the data set varied form one station to another ranging from 990 to 6684 patterns, and the detail for each station was provided in Table 1. For each station, the dataset was randomly divided into two subgroups: one for the calibration period (70%) and the rest (30%) for validation. Table 2 reported the mean, maximum, minimum, standard deviation, coefficient of variation values, and the coefficient of correlation with TU, i.e., X_{mean}, X_{max}, X_{min}, S_x, C_v, and R, respectively.

TABLE 1 Period of records for the USGS stations selected for Modeling River turbidity.

Station	Begin date	End date	Total patterns	Incomplete patterns	Final patterns
USGS 1497500	01/11/2007	31/12/2015	2983	1993	990
USGS 11501000	16/11/2007	02/09/2020	4675	711	3964
USGS 14210000	01/07/2001	03/09/2020	7005	321	6684
USGS 14211010	01/06/2002	03/09/2020	6670	229	6441

TABLE 2 Summary statistics of water quality variables for the four stations.

Variables	Subset	Unit	X_{mean}	X_{max}	X_{min}	S_x	C_v	R
USGS 11497500 Sprague River near Beatty, Klamath Basin, Oregon, United States								
TU	Training	FNU	7.306	47.700	1.900	7.376	1.010	1.000
	Validation	FNU	6.937	45.600	1.900	6.843	0.986	1.000
	All data	FNU	7.196	47.700	1.900	7.221	1.003	1.000
Q	Training	Kcfs	313.386	1500.000	82.600	264.966	0.845	0.503
	Validation	Kcfs	310.379	1520.000	82.800	270.773	0.872	0.531
	All data	Kcfs	312.486	1520.000	82.600	266.653	0.853	0.510
USGS 11501000 Sprague River near Chiloquin, Klamath Basin, Oregon, United States								
TU	Training	FNU	7.239	78.400	0.500	8.614	1.190	1.000
	Validation	FNU	7.407	63.700	0.500	8.483	1.145	1.000
	All data	FNU	7.290	78.400	0.500	8.575	1.176	1.000
Q	Training	Kcfs	477.993	4430.000	100.000	482.665	1.010	0.548
	Validation	Kcfs	501.307	4380.000	101.000	531.828	1.061	0.562
	All data	Kcfs	484.984	4430.000	100.000	497.999	1.027	0.552
USGS 14210000 Clackamas River at Estacada, Oregon, United States								
TU	Training	FNU	2.225	75.400	0.000	4.692	2.109	1.000
	Validation	FNU	2.524	78.300	0.000	5.575	2.209	1.000
	All data	FNU	2.314	78.300	0.000	4.975	2.149	1.000
Q	Training	Kcfs	2540.357	24800.000	589.000	2252.682	0.887	0.740
	Validation	Kcfs	2635.124	28900.000	601.000	2371.804	0.900	0.746
	All data	Kcfs	2568.781	28900.000	589.000	2289.388	0.891	0.741
USGS 14211010 Clackamas River near Oregon City, Oregon, United States.								
TU	Training	FNU	3.088	100.000	0.000	6.390	2.069	1.000
	Validation	FNU	3.144	93.800	0.000	6.814	2.167	1.000
	All data	FNU	3.105	100.000	0.000	6.520	2.100	1.000
Q	Training	Kcfs	3270.327	27500.000	630.000	3115.037	0.953	0.784
	Validation	Kcfs	3265.621	32600.000	624.000	3312.813	1.014	0.811
	All data	Kcfs	3268.915	32600.000	624.000	3175.539	0.971	0.793

X_{mean}, mean; X_{max}, maximum; X_{min}, minimum; S_x, standard deviation; C_v, coefficient of variation; R, coefficient of correlation with TU; *TU*, water turbidity; *Q*, discharge; *FNU*, Formazin Nephelometric Unit; *Kcfs*, thousand cubic feet per second.

3. Methodology

3.1 Feedforward artificial neural network

Artificial neural networks (ANN) are widely used for solving a large number of problems in the area of water resources management and now becoming a successful tool for tackling complex and nonlinear problem (Olyaie et al., 2017; Mehr and Nourani, 2018; Hrnjica et al., 2019; Matouq et al., 2013). The success of the ANN in comparison to other regression models was primarily due to their ability to adapt and to be flexible in extracting the nonlinear relationship between variables using a learning process (Haykin, 1999). There is a large number of the ANN architecture; however, the FFNN is the

most and widely used model in the literature. As the name suggests, the FFNN is composed of several layers: input layer, hidden layers, and output layer, and generally only one hidden layer is adopted, and the available information spreads through the network from the input to the output layer. The input layer contains the independent variables (x_1, x_2, x_3, …, x_i), the hidden layer is composed of several neurons determined by trial and error, and each one receives the all input variables (x_i) multiplied by their respective parameters (the weights), use a summation function and added one bias to the results. The output of each hidden neuron was produced using an activation function, generally the sigmoidal function. Finally, the output layer sums the weighted output of the hidden neurons and uses a linear transfer function to provide the final output response. The weights and biases of the ANN models will be adjusted during the training process to minimize a cost function, generally the sum of squares error calculated as the differences between the measured and predicted value. The well-known and widely used training algorithm is the back propagation (Haykin, 1999).

3.2 Dynamic evolving neural-fuzzy inference system

Evolving neural-fuzzy inference systems are intelligent models with high similarity with the classical neuro-fuzzy approaches for which the linear and nonlinear parameters were adopted in an online manner, more precisely; the nonlinear parameters were governed by the kind of partition of the input-output space (Škrjanc et al., 2019). DENFIS is the most relevant evolving system introduced during the last decade (Kasabov and Song, 2002) and is mainly based on the so-called evolving clustering method (Heddam and Kisi, 2020; Kasabov et al., 2008). From a computational point of view, the DENFIS model can be run in two manners namely the online and the offline. The first the version is based on the online training method and the model is called DENFIS_ON, while the second method is based on the offline training method and the model is called DENFIS_OF (Kasabov and Song, 2002; Kasabov et al., 2008). The triangular fuzzy membership functions are used for both online and offline DENFIS models:

$$\mu(x) = mf(x, a, b, c) = \begin{cases} 0, & x \le a \\ \dfrac{x-a}{b-a}, & a \le x \le b \\ \dfrac{c-x}{c-b}, & b \le x \le c \\ 0. & c \le x \end{cases} \tag{1}$$

where b is the value of the cluster center on the x dimension, $a = b - d \times Dthr$ and $c = b + d \times Dthr$, $d = 1.2 \div 2$; the distance threshold value, $Dthr$, is a clustering parameter (Kasabov and Song, 2002; Kasabov et al., 2008; Heddam et al., 2018). During the last few years, DENFIS models have been applied for solving several engineering problems, and more details related to its application can be found in Adnan et al. (2021), Sebbar et al. (2020), Heddam and Kisi (2020), Heddam et al. (2018), Kisi et al. (2019a,b). The MatLab software for DENFIS can be found in https://kedri.aut.ac.nz/areas-of-expertise/data-mining-and-decision-support/neucom.

3.3 Bat algorithm optimized extreme learning machine

Single hidden layer feedforward neural network (SLFN) is the most and relevant ANN model proposed during the last decades, not only regarding its simplicity, i.e., having only one hidden layer, but also in regards to its robustness, high precision, and universal approximation capability. With the invention of the back-propagation training algorithm, the SLFN had become famous (Hornik et al., 1989; Hornik, 1991). From a computational point of view, the back-propagation is used for iteratively updating all SLFN parameters (i.e., weights and biases) from the input to the output layers, bringing the total number of updated parameters high, and in some cases (i.e., large data set) the training process become very slow and suffer from the overfitting problem. In order to meet these challenges, a new training algorithm called extreme learning machine (ELM) was arriving (Huang et al. 2006a,b), such that the weights between the input and hidden layer are obtained directly and do not need to be updated during the training process, which is called the random generation of the hidden nodes, while those linking the hidden to the output layers were analytically determined. According to Huang et al. (2006a,b), SLFN with N hidden layer nodes can be expressed as follows:

$$Y_j = \sum_{i=1}^{N} \beta_i \psi\left(w_i \cdot x_j + b_i\right) \quad j = 1,\ldots M \tag{2}$$

where M is the number of training simple, N is the number of hidden nodes, w_i is a single input to hidden layers weight, Ψ is the activation function, β_i is hidden to output layers weights, b_i is the hidden nodes biases, x_j correspond to the input variables matrix. The mathematical formulation of the ELM approach could be described as:

$$H\beta = T \tag{3}$$

where H is the hidden layer output matrix, β is the weight matrix of the output layer, and T is the expected output matrix (Liu et al., 2020a; Cheng et al., 2020).

Several metaheuristics training algorithms have been proposed during the last few years for improving the training process of the ANN and ELM models, among them: genetic algorithm (GA), particle swarm optimization (PSO), bee colony (ABC) optimization algorithm, Ant Colony Optimization (ACO), differential evolution (DE), and cuckoo search algorithm (CSA). In the present study, an efficient optimization method called Bat optimization was introduced to optimize the ELM model and described later.

The Bat optimization algorithm introduced by Yang (2010) is a metaheuristics approach belonging into the category of swarm intelligence models, and it was inspired by the behavior by which the bats seek their prey with a special sense (Jaddi et al., 2015). The main idea behind the bat algorithm is mainly based on the echolocation capability and social behavior of the bat population (Xie et al., 2019). From a computational point of view the bat algorithm possesses the following three idealized rules (Shekhar et al., 2020; Liu et al., 2020b):

- **(i)** The echolocation is used by the bats as a method to calculate and to know the relative distance from a food source and obstacles in an unknown way.
- **(ii)** In order to search the prey, an initial velocity V_i should be randomly assigned at a starting position X_i. The bats fly at the same relative velocity for different times due to different initial distances, using a fixed frequency f_i ranging between two limits $f_{\min}$ and $f_{\max}$, varying wavelength λ and the loudness or sound intensity A_0. According to the level of proximity to the target, the bat automatically adjusts the wavelength and pulse rate accordingly.
- **(iii)** Ranging from a maximum (A_0) to a minimum ($A_{\min}$), the loudness of the pulse should be adjusted accordingly.

The output of this iterative process is achieved according to a series of iterations according to a large number of available solutions, in which the loudness and pulse rate were updated in response to the received accepted solution. Consequently, the frequency, velocity, and position values of any bat member are calculated as follow (Gangwar and Pathak, 2020):

$$f_i = f_{\min} + (f_{\max} - f_{\min})\beta \tag{4}$$

$$V_i^t = V_i^{t-1} + \left(X_i^{t-1} - X_{\text{best}}^t\right) f_i \tag{5}$$

$$X_i^t = X_i^{t-1} + V_i^t \tag{6}$$

where β ranging is a random number ranging from 0 to 1, f_i ranging from $f_{\min}$ to $f_{\max}$ denoted as the frequency and used for controlling the step length (i.e., the step and range) of the bat movement, and it corresponds to a range of wavelengths [$\lambda_{\min}$, $\lambda_{\max}$], and X_{best} is the global best solution. During the iteration process, the updated solution is calculated a follow (Gangwar and Pathak, 2020):

$$X_{\text{new}} = X_{\text{old}} + \varepsilon A^t \tag{7}$$

where ε is a random number ranging between zero and one [0, 1], and A^t represents the average value of Bats loudness at the time t. Flowchart of the developed Bat-ELM model is shown in Fig. 2. The MatLab code of the Bat algorithm can be found in https://fr.mathworks.com/matlabcentral/fileexchange?q=Bat+algorithm.

3.4 Multiple linear regression

Using the MLR method, one dependent variable Y (in our study the river turbidity) is linked or correlated with several predictor variables x_i, using the following equation (Luu et al., 2021):

$$Y_i = \beta_0 + \sum_{i=1}^{K} \beta_i x_i + e_i \tag{8}$$

where β_0 is the intercept, β_i were the partial regression coefficients for each predictor and the e is the residual.

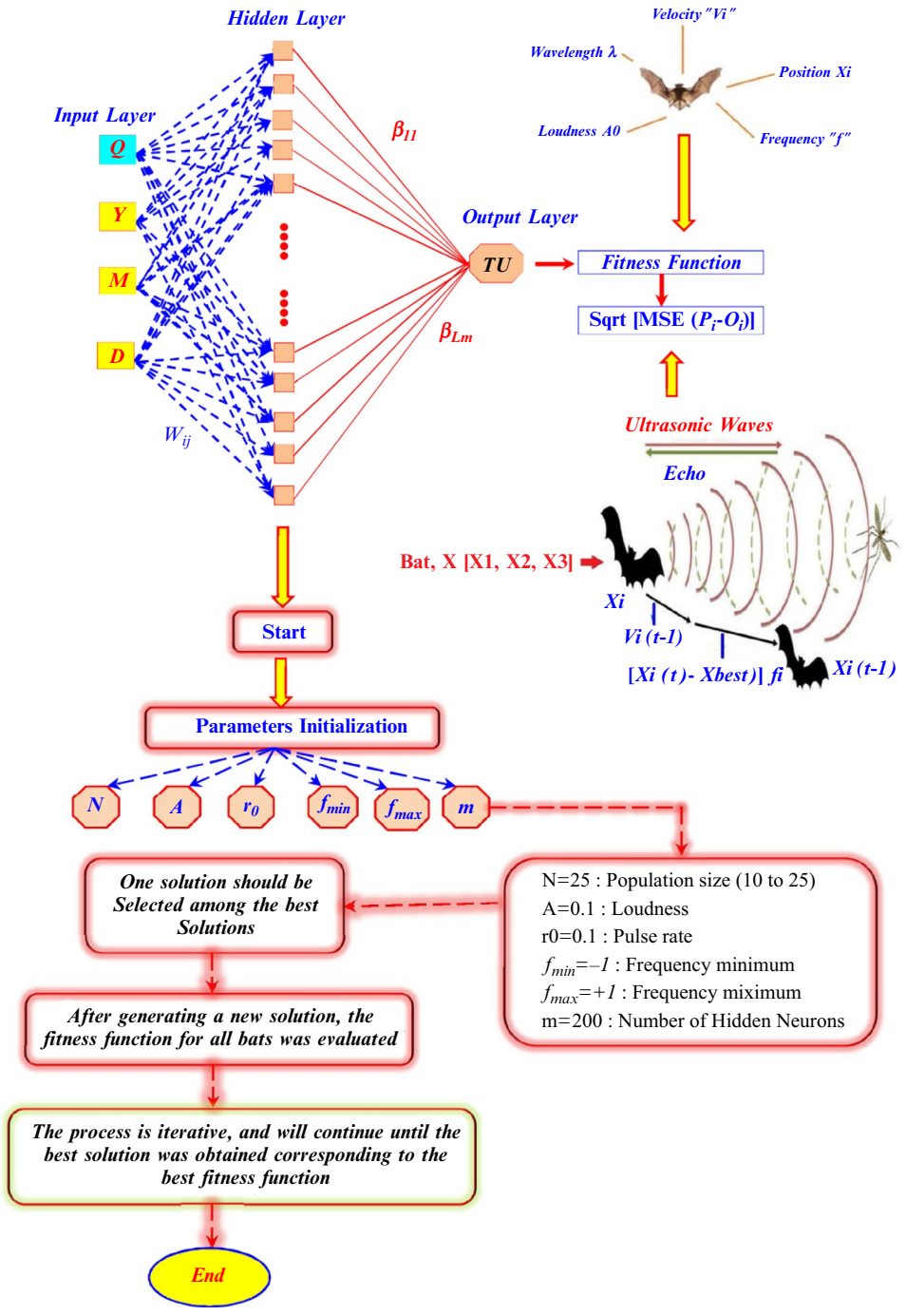

FIG. 2 Extreme learning machines optimized Bat algorithm flowchart.

3.5 Performance assessment of the models

In the present chapter, the performances of the proposed models were evaluated using: coefficient of correlation (R), Nash-Sutcliffe efficiency (NSE), mean absolute error (MAE), and root mean square error (RMSE) are calculated as follow:

$$\mathrm{MAE} = \frac{1}{N}\sum_{i=1}^{N}\left|(TU_0)_i - \left(TU_p\right)_i\right|, \quad (0 \le \mathrm{MAE} < +\infty) \tag{9}$$

$$\mathrm{RMSE} = \sqrt{\frac{1}{N}\sum_{i=1}^{N}\left[(TU_0)_i - \left(TU_p\right)_i\right]^2}, \quad (0 \le \mathrm{RMSE} < +\infty) \tag{10}$$

$$\mathrm{NSE} = 1 - \left[\frac{\sum_{i=1}^{N}\left[(TU_0)_i - (TU_p)_i\right]^2}{\sum_{i=1}^{N}\left[(TU_0)_i - \overline{TU}_0\right]^2}\right], \quad (-\infty < \mathrm{NSE} \leq 1) \tag{11}$$

$$R = \left[\frac{\frac{1}{\mathrm{N}}\sum_{i=1}^{N}\left((TU_0)_i - TU_0\right)\left((TU_p)_i - \overline{TU}_p\right)}{\sqrt{\frac{1}{\mathrm{N}}\sum_{i=1}^{n}\left((TU_0)_i - \overline{TU}_0\right)^2}\sqrt{\frac{1}{\mathrm{N}}\sum_{i=1}^{n}\left((TU_p)_i - \overline{TU}_p\right)^2}}\right], \quad (-1 < R \leq +1) \tag{12}$$

In which, N is the number of data, TU_0, TU_p, $\overline{TU}_0$, $\overline{TU}_p$ are the measured, predicted, mean measured, and mean predicted river water turbidity, respectively.

4. Results and discussion

As stated above, the goal of our study was the prediction of river turbidity at four rivers located in the United States. For this purpose, four machine learning models were developed and compared according to two scenarios: (i) using the river discharge (Q) and the periodicity (i.e., year, month, and day) numbers, and (ii) using only river discharge. The RMSE, MAE, R, and NSE, respectively, were calculated during the training and validation phases separately, and the obtained results were further analyzed using graphical representations. Overall, at the four stations, the river TU were poorly estimated using only river Q compared to the estimation achieved using Q and the periodicity, and the Bat-ELM showed the best correlation among all proposed models over the four stations. Detailed results for each station are discussed hereafter.

4.1 USGS 1497500 station

The numerical results of daily river TU prediction at the USGS 1497500 station using the four machine learning models are illustrated in Table 3. According to Table 3, using only the Q as an input variable, the DENFIS_O2, DENFIS_F2, FFNN2, and Bat-ELM2 models exhibit small variations during the validation phase, and none of them was able to correctly and accurately predict TU concentration. The RMSE and MAE values ranging from 5.593 to 6.230 and 3.256 to 3.575, respectively, show the poor models performances during the validation stage. The NSE and R values were very low and do not exceed 0.331 and 0.576, respectively. However, inclusion of the periodicity guaranteed a significant improvement in the models performances for all proposed models. The river TU retrieved has a NSE coefficient of no <0.660 for all models and the R values were superior to 0.827. In addition, the RMSE and MAE values were no more than 3.99 and 2.26, respectively. These results imply that the four machine learning models have been able to predict the river TU very accurately by the inclusion of the periodicity. Overall, the best accuracy was obtained using the Bat-ELM1 with R and NSE of 0.972 and 0.936, respectively, versus 0.905 and 0.770 for FFNN1, and 0.850 and 0.708 for DENFIS_O1, significantly higher than the

TABLE 3 Performances of different River Turbidity models at the USGS 11497500 station.

	Training				Validation			
Models	R	NSE	RMSE	MAE	R	NSE	RMSE	MAE
Bat-ELM1	0.984	0.968	1.314	0.894	0.972	0.936	1.731	1.155
Bat-ELM2	0.596	0.355	5.919	3.684	0.576	0.331	5.593	3.256
DENFIS_O1	0.924	0.593	4.704	2.948	0.850	0.708	3.694	2.023
DENFIS_O2	0.916	0.364	5.876	3.630	0.530	0.170	6.230	3.575
DENFIS_F1	0.842	0.657	4.316	2.425	0.827	0.659	3.992	2.258
DENFIS_F2	0.573	0.294	6.191	4.044	0.564	0.278	5.809	3.503
FFNN1	0.979	0.959	1.490	0.964	0.905	0.770	3.276	1.787
FFNN2	0.638	0.408	5.673	3.563	0.500	0.225	6.018	3.468

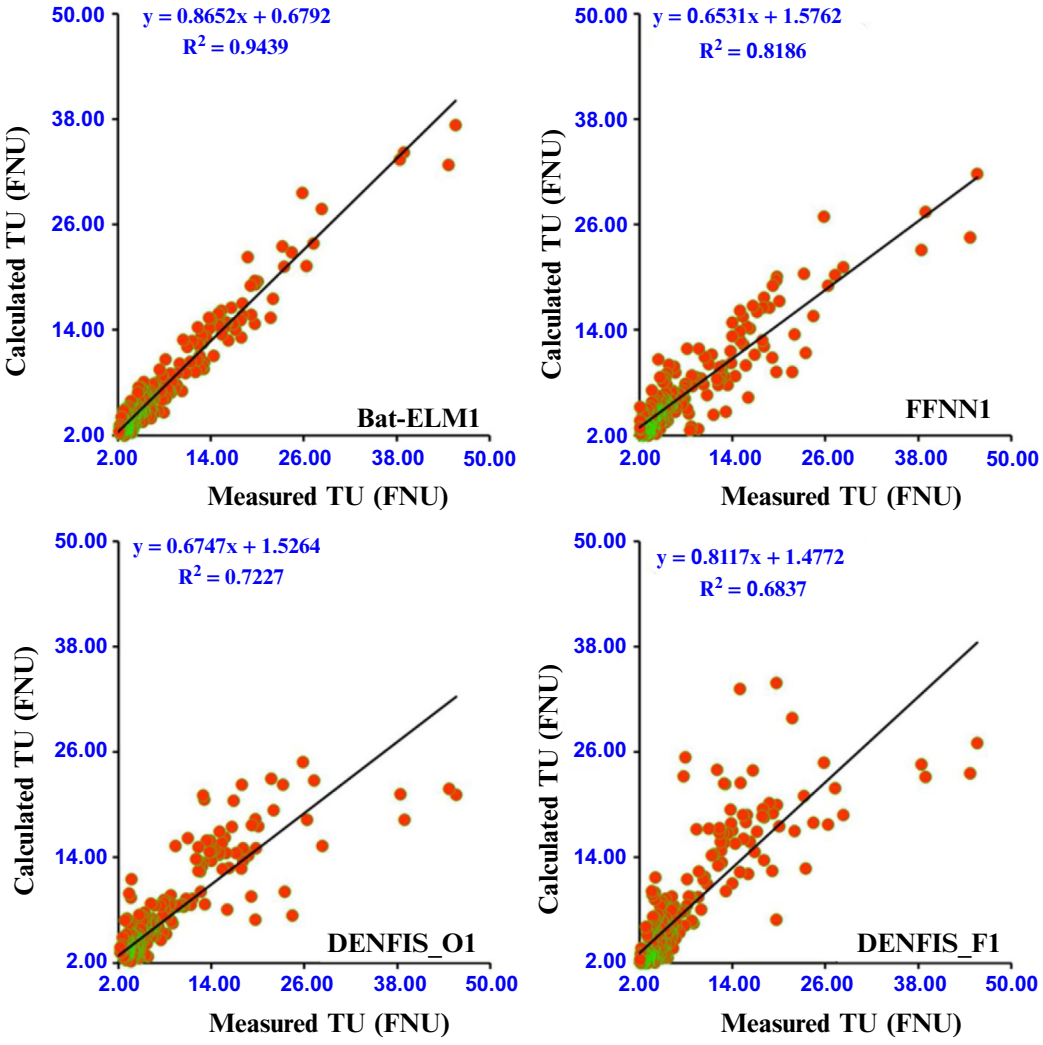

FIG. 3 Scatterplots of measured against calculated Turbidity at the USGS 11497500 station.

weakest performances obtained using the DENFIS_F1 model with *R* and NSE values of 0.827 and 0.659, respectively, which is still largely less than the other three models. In addition, the Bat-ELM1 improves the FFNN1, DENFIS_O1, and DENFIS_F1 by 47.16% and 35.37%, 53.14% and 42.19%, and 56.64% and 48.85% reduction in terms of RMSE and MAE, respectively. Clearly, Bat-ELM1, FFNN1, and DENFIS_O1 were more accurate compared to DENFIS_F1, and Bat-ELM1 further improves the river TU estimation. Fig. 3 shows scatterplot of river TU values calculated by DENFIS_O1, DENFIS_F1, FFNN1, and Bat-ELM1 models compared with in situ measurement. A first look at the results reveals high-to-moderate agreement between calculated and measured data by all four algorithms. However, it may seem that the Bat-ELM1 possess the high accuracy with very low scattered data, followed by the FFNN1, the DENFIS_O1 in the third place, while the high scattered data were obtained using the DENFIS_F1.

4.2 USGS 11501000 station

River TU estimation at the USGS 115001000 using the four machine learning models are compared to the in situ measured data in Fig. 4 for the validation dataset. For both Bat-ELM1 and FFNN1 models, simulated TU fall generally along the one to one line against in situ measurements with less scattered data and the superiority of the Bat-ELM1 is obvious; however, the DENFIS_O1 and DENFIS_F1 worked equally with slight difference, and they are less accurate compared to Bat-ELM1 and FFNN1 with large scattered data. Quantitative measures of all river TU comparisons are shown in Table 4 in terms of RMSE, MAE, NSE, and *R* values. From Table 4, estimated river TU was poorly correlated with in situ measured data for the models based only on river discharge. The four machine learning models have low NSE and *R* values ranging from 0.384 to

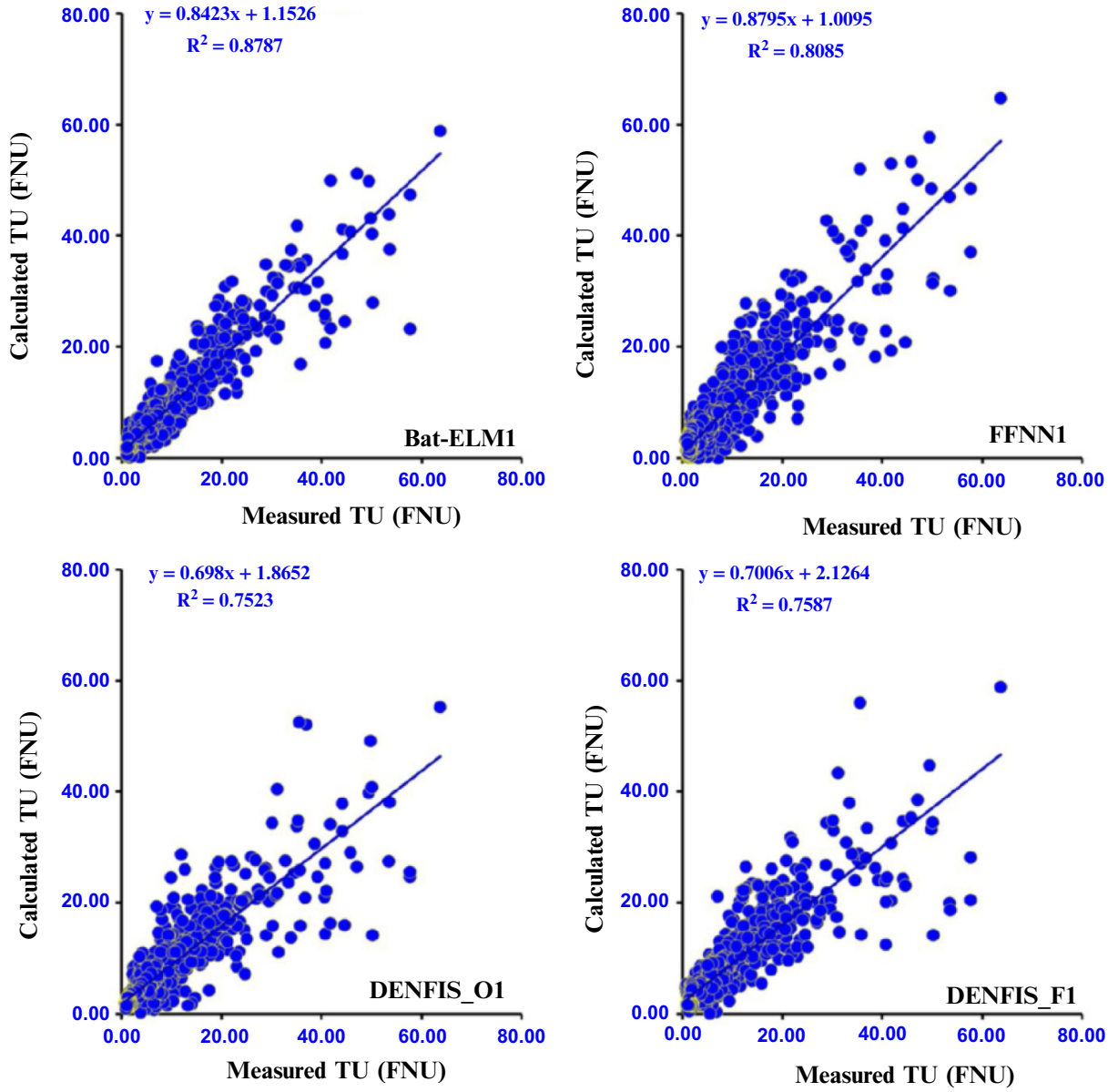

FIG. 4 Scatterplots of measured against calculated Turbidity at the USGS 11501000 station.

TABLE 4 Performances of different River Turbidity models at the USGS 11501000 station.

	Training				Validation			
Models	*R*	NSE	RMSE	MAE	*R*	NSE	RMSE	MAE
Bat-ELM1	0.941	0.885	2.921	1.582	0.937	0.877	2.972	1.748
Bat-ELM2	0.685	0.469	6.273	3.217	0.699	0.488	6.069	3.295
DENFIS_O1	0.868	0.705	4.680	1.836	0.867	0.746	4.271	2.174
DENFIS_O2	0.720	0.478	6.224	2.984	0.656	0.384	6.657	3.617
DENFIS_F1	0.877	0.764	4.187	2.101	0.871	0.754	4.206	2.250
DENFIS_F2	0.677	0.458	6.340	3.338	0.702	0.490	6.054	3.408
FFNN1	0.981	0.963	1.667	1.103	0.899	0.802	3.773	2.376
FFNN2	0.725	0.525	5.933	3.050	0.664	0.437	6.362	3.436

0.490 and from 0.656 to 0.702, respectively, and none of the models possess a NSE value greater than 0.50. In terms of errors metrics, the obtained RMSE and MAE were very high ranging from 6.054 to 6.657 and from 3.408 to 3.617, respectively. The difference in models performances between scenario 1 and 2 is apparent and the significant contribution of the periodicity in the improvement of the models accuracy was completely clear for which the NSE and *R* value are somewhat larger and the RMSE and MAE values are somewhat small. The RMSE and MAE of the Bat-ELM1 and FFNN1 were improved by 51.03% and 46.95%, 40.69% and 30.85%, respectively. In addition, the RMSE and MAE of the DENFIS_O1 and DENFIS_F1 were improved by 35.84% and 39.89%, 30.53% and 33.98%, respectively. The most significant improvement was achieved using the Bat-ELM1 for which the RMSE had dropped from 6.069 to 2.972, while the MAE value was decreased from 3.295 to 1.748, respectively. In addition, an increase in the NSE and *R* values is to be expected: the *R* spiked to almost 0.937 compared to 0.699 (25.40% improvement) obtained using only the river discharge, while the NSE value rose by 44.36% (0.488–0.877). The improvement on models accuracies was attributed to the introduction of the periodicity as input variable combined the discharge. Finally, comparison between the models accuracy revealed the superiority of the Bat-ELM1, followed by the FFNN1, while the two DENFIS models have typically the same performances. For comparison, Bat-ELM1 decreased the RMSE and MAE values of the FFNN1, DENFIS_O1, and DENFIS_F1 by 21.23% and 26.43%, 30.41% and 19.60%, and 29.34% and 22.31%, respectively.

4.3 USGS 14210000 station

Table 5 shows the numerical results obtained at the USGS 14210000 station using the machine learning models described above. During the validation phase, the minimum RMSE and MAE of the second scenario (i.e., using only *Q*) are given as well as the NSE and *R* values, showing the superiority of the Bat-ELM2 model, while the FFNN2, DENFIS_O2, and DENFIS_F2 exhibit relatively the same level of accuracies, for which statistical measurement of error, i.e., RMSE and MAE showed a range of 3.185–3.753, and 1.244–1.334, respectively, with larger errors values obtained by the FFNN2 (RMSE = 3.753, MAE = 1.334).

From Table 5, it can be seen that the errors index calculated using the Bat-ELM2 are generally the lower one with RMSE and MAE of 3.185 FNU and 1.245 FNU, respectively. Across the two scenarios with and without the periodicity, scenario 1 having the *Q* and the periodicity as input variables show better performances over the four machine learning models, with measurement errors (i.e., RMSE and MAE) significantly reduced. The RMSE varies from 3.396 at worst to 2.456 at best, and the MAE varies from 1.299 at worst to 1.117 at best. Quantitative comparisons for all models in the form of RMSE, MAE, *R*, and NSE values between observed and simulated values reported in Table 5 revealed that a significant percentage improvement was achieved using the Bat-ELM1 in comparison to the FFNN1, DENFIS_O1, and DENFIS_F1 models. The Bat-ELM1 increased *R* and NSE values by 9.24% and 23.43%, and decreased RMSE and MAE values by 25.21% and 14.01%, respectively, in the validation phase, compared to the FFNN1 model. In addition, The Bat-ELM1 decreased the RMSE and MAE values by 27.68% and 7.76%, and increased *R* and NSE values by 11.97% and 28.14%, respectively, in the validation phase, compared with DENFIS_O1 model. Finally, the Bat-ELM1 was more accurate compared to DENFIS_F1 showing a significant decrease of the RMSE and MAE by 25.213% and 14.011%, respectively.

TABLE 5 Performances of different River Turbidity models at the USGS 14210000 station.

	Training				Validation			
Models	*R*	NSE	RMSE	MAE	*R*	NSE	RMSE	MAE
Bat-ELM1	0.850	0.723	2.469	1.109	0.898	0.806	2.456	1.117
Bat-ELM2	0.831	0.691	2.607	1.042	0.821	0.674	3.185	1.245
DENFIS_O1	0.808	0.594	2.989	1.160	0.802	0.629	3.396	1.211
DENFIS_O2	0.835	0.664	2.718	0.959	0.799	0.623	3.420	1.244
DENFIS_F1	0.898	0.804	2.075	0.901	0.807	0.646	3.318	1.241
DENFIS_F2	0.821	0.674	2.677	1.040	0.790	0.625	3.415	1.277
FFNN1	0.901	0.812	2.036	0.935	0.822	0.653	3.284	1.299
FFNN2	0.856	0.733	2.424	0.996	0.771	0.547	3.753	1.334

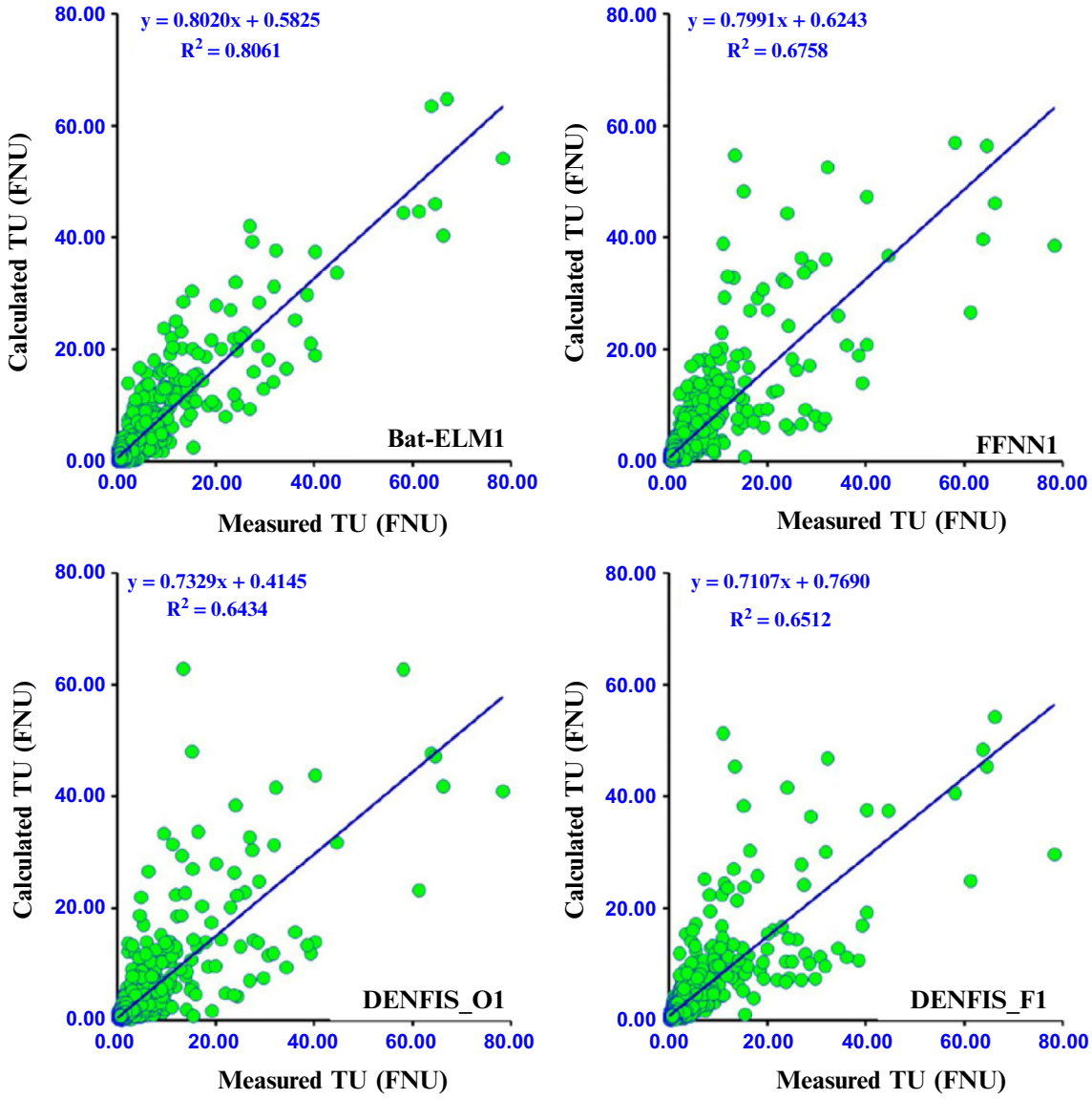

FIG. 5 Scatterplots of measured against calculated Turbidity at the USGS 14210000 station.

The comparisons between simulated and in situ measured TU are given in Fig. 5 in terms of scatterplot. The agreement is very good for Bat-ELM1 with R^2 determination coefficient always above 0.80, and the data were less scattered in comparison to the other three models for which the data were largely scattered with an R^2 approaching 0.670.

4.4 USGS 14211010 station

At the USGS 14211010 station (Table 6), for the four developed models, it can be concluded that both during the training and the validation phase, results showed that the inclusion of the periodicity as input variable has a marked effect on the performances of the models. During the validation phase, it is clear from the obtained results that using only the river discharge as input variable, the performances of FFNN2, Bat-ELM2, DENFIS_O2, and DENFIS_F2 models were relatively similar with slight superiority in favor to DENFIS_F2. An analysis of the statistical indices shows that the R and NSE values are in the range of 0.824–0.852 and 0.679–0.726. Similarly, the RMSE and MAE range from 3.56 to 3.86 FNU and from 1.338 to 1.407, respectively. From Table 6, it is clear that the inclusion of the periodicity improves the performances of both models. Using the periodicity and Q as input variables, the best Bat-ELM1 model had RMSE = 2.626, MAE = 1.161, $R = 0.923$, and NSE = 0.851, and surpasses all other models in terms of accuracy. Scatterplot of calculated versus measured river TU are given in Fig. 6. Finally, the performances of the models were evaluated and compared in terms of boxplot (Fig. 7) and Taylor diagram (Fig. 8) showing the superiority and the high performances of the Bat-ELM1 compared to the all developed models.

TABLE 6 Performances of different River Turbidity models at the USGS 14211010 station.

Models	Training				Validation			
	R	NSE	RMSE	MAE	*R*	NSE	RMSE	MAE
Bat-ELM1	0.934	0.872	2.289	1.145	0.923	0.851	2.626	1.161
Bat-ELM2	0.837	0.700	3.500	1.385	0.844	0.708	3.682	1.430
DENFIS_O1	0.867	0.727	3.336	1.289	0.862	0.739	3.480	1.422
DENFIS_O2	0.869	0.747	3.216	1.313	0.837	0.698	3.744	1.338
DENFIS_F1	0.931	0.867	2.329	1.062	0.847	0.704	3.705	1.226
DENFIS_F2	0.880	0.774	3.039	1.317	0.852	0.726	3.564	1.345
FFNN1	0.945	0.893	2.093	1.031	0.827	0.638	4.097	1.249
FFNN2	0.891	0.793	2.904	1.303	0.824	0.679	3.862	1.407

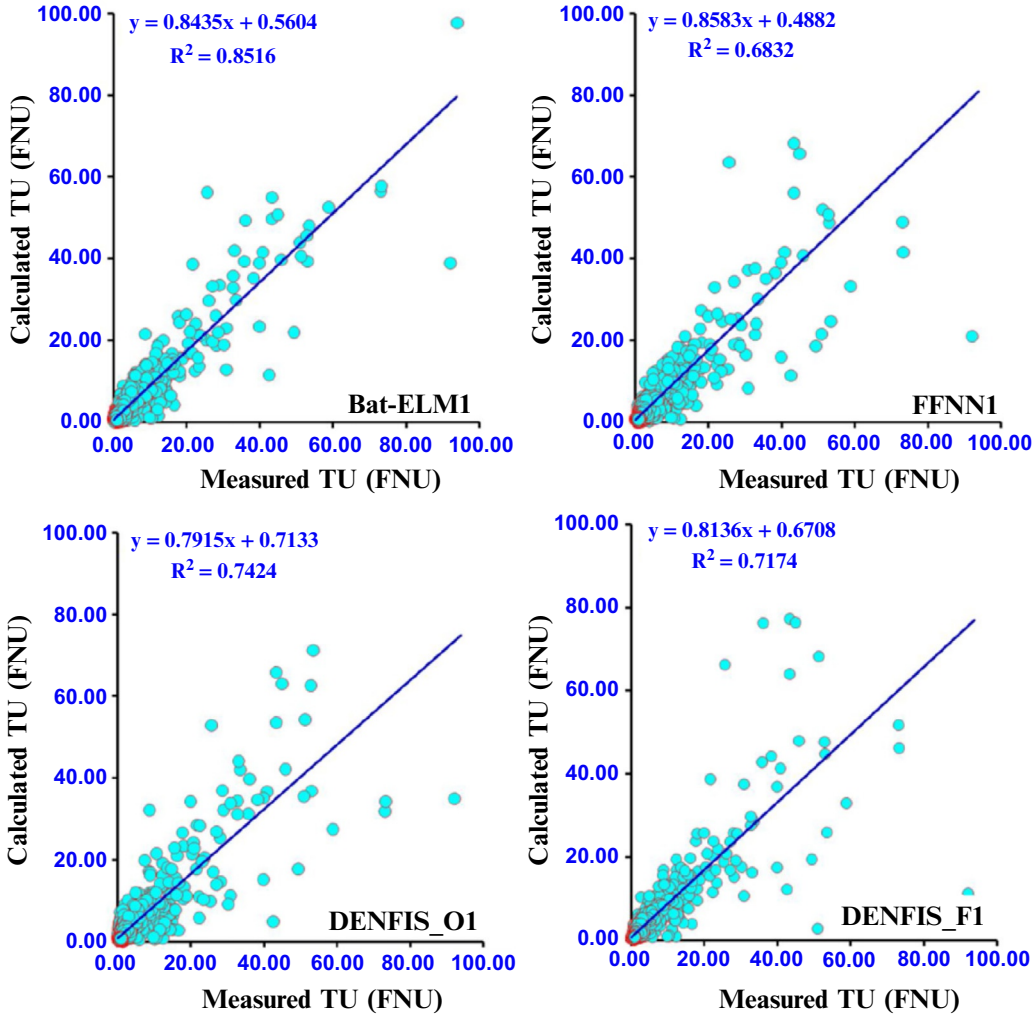

FIG. 6 Scatterplots of measured against calculated Turbidity at the USGS 14211010 station.

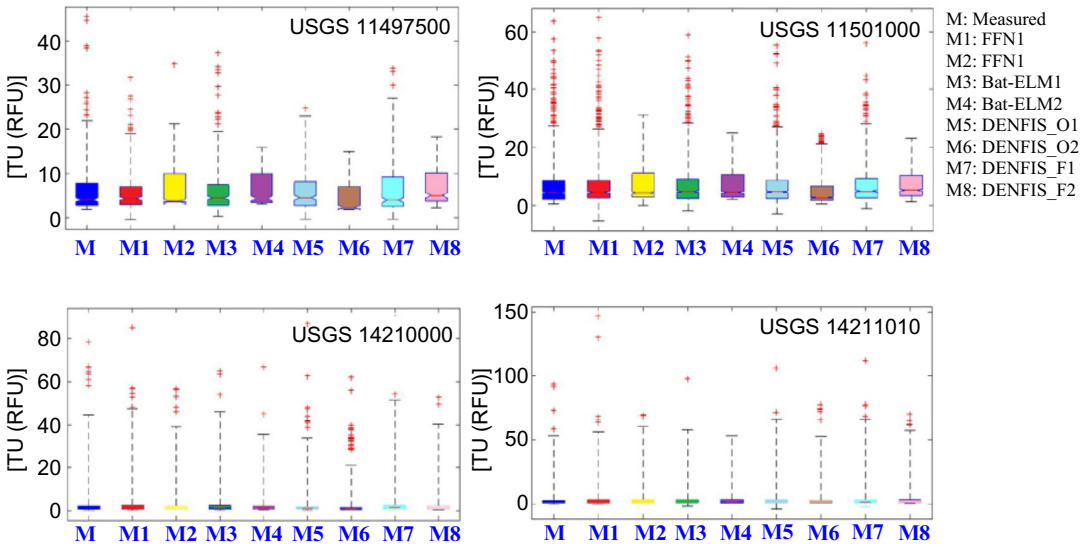

FIG. 7 Box-plots of measured and calculated river turbidity (TU: RFU) for the four USGS stations. Boxes are generated using validation dataset illustrating the 25th and 75th percentiles, and the median. Whiskers include the highest and lowest values and the mean values are marked by *red line*.

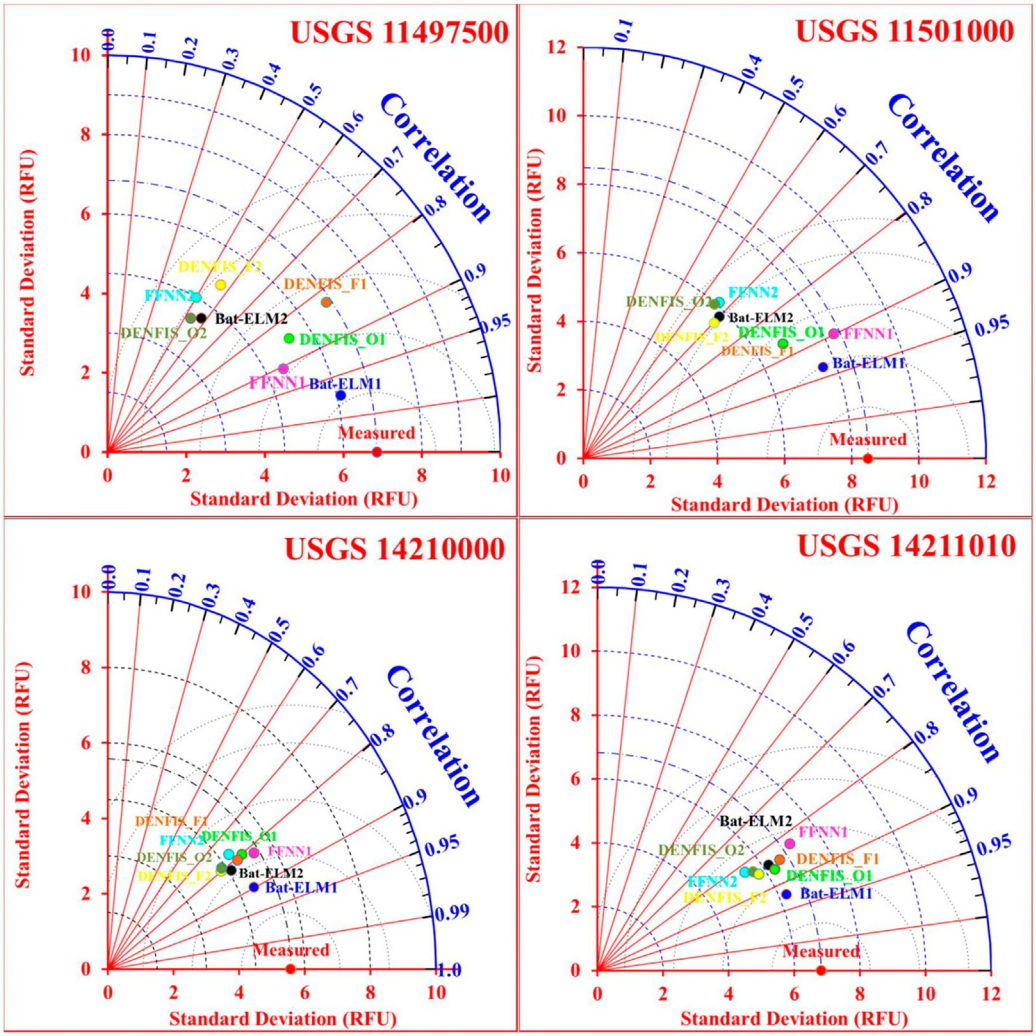

FIG. 8 Taylor diagram of river turbidity (TU: RFU) illustrating the statistics of comparison between the proposed models at the four USGS stations.

5. Conclusions

As a key water quality variable, river turbidity is of great concern in a large number environmental, water resources, and hydrological studies. In this study, first, a robust model for predicting the river TU using only river discharge was fitted and the obtained results were low to moderate. Next, a nonlinear model between the river TU, discharge, and the periodicity (i.e., day, month, and year numbers) was established using a new hybrid machine learning model (i.e., Bat-ELM). Then, the proposed model was applied and tested using data collected at four USGS stations. And finally, the estimation provided by the Bat-ELM was compared to those achieved using two kinds of machine learning models namely the FFNN and DENFIS models. The new method introduced in the present study (Bat-ELM) made a good to excellent work, and an excellent progress in modeling the river TU was achieved. Therefore, the new method was defined as the best and the useful method for the estimation of the river TU. The overall accuracy of prediction was significantly improved by the inclusion of the periodicity and the correlation coefficient between the measured and predicted river TU reached 0.97, and the corresponding RMSE was 1.731. However, when the model was examined without the inclusion of the periodicity and using only the river discharge, the performances of the Bat-ELM were not the greatest and in some cases, it was surpassed by the DENFIS models. Results obtained in the present study encompass an encouraging record of progress and achievement by the use of the machine learning models, and can be applied using data from other stations. Future work should be emphasized on performances of the proposed models using other input variables and future researches should be encouraged. Also, the obtained results in the present chapter seem to be interesting and the overall merits of the proposed hybrid Bat-ELM highlighted. Having seen that, the Bat-ELM surpasses all of the FFNN and DENFIS models at the four stations has lead us to conclude that the idea of hybridizing machine learning, i.e., the ELM is very promising and should be used for the other machine learning models.

References

Adnan, R.M., Liang, Z., Parmar, K.S., Soni, K., Kisi, O., 2021. Modeling monthly streamflow in mountainous basin by MARS, GMDH-NN and DENFIS using hydroclimatic data. Neural Comput. Applic. 33 (7), 2853–2871.

Allam, M., Khan, M.Y.A., Meng, Q., 2020. Retrieval of turbidity on a spatio-temporal scale using Landsat 8 SR: a case study of the Ramganga River in the Ganges Basin, India. Appl. Sci. 10 (11), 3702. https://doi.org/10.3390/app10113702.

Al-Yaseri, I., Morgan, S., Retzlaff, W., 2013. Using turbidity to determine total suspended solids in storm-water runoff from green roofs. J. Environ. Eng. 139 (6), 822–828. https://doi.org/10.1061/(ASCE)EE.1943-7870.

Cheng, K., Gao, S., Dong, W., Yang, X., Wang, Q., Yu, H., 2020. Boosting label weighted extreme learning machine for classifying multi-label imbalanced data. Neurocomputing 403, 360–370. https://doi.org/10.1016/j.neucom.2020.04.098.

Gangwar, S., Pathak, V.K., 2020. Dry sliding wear characteristics evaluation and prediction of vacuum casted marble dust (MD) reinforced ZA-27 alloy composites using hybrid improved bat algorithm and ANN. Mater. Today Commun. 25, 101615. https://doi.org/10.1016/j.mtcomm.2020.101615.

Gelda, R.K., Effler, S.W., 2007. Modeling turbidity in a water supply reservoir: advancements and issues. J. Environ. Eng. 133 (2), 139–148. https://doi.org/10.1061/(ASCE)0733-9372(2007)133:2(139).

Gelda, R.K., Effler, S.W., Peng, F., Owens, E.M., Pierson, D.C., 2009. Turbidity model for Ashokan Reservoir, New York: case study. J. Environ. Eng. 135 (9), 885–895. https://doi.org/10.1061/(ASCE)EE.1943-7870.0000048.

Gelda, R.K., Effler, S.W., Prestigiacomo, A.R., Peng, F., Effler, A.J., Wagner, B.A., et al., 2013. Characterizations and modeling of turbidity in a water supply reservoir following an extreme runoff event. Inland Waters 3 (3), 377–390. https://doi.org/10.5268/IW-3.3.581.

Gu, K., Zhang, Y., Qiao, J., 2020. Random forest ensemble for river turbidity measurement from space remote sensing data. IEEE Trans. Instrum. Meas. https://doi.org/10.1109/TIM.2020.2998615.

Haykin, S., 1999. Neural Networks a Comprehensive Foundation. Prentice Hall, Upper Saddle River, UK.

Heddam, S., Kisi, O., 2020. Evolving connectionist systems versus neuro-fuzzy system for estimating total dissolved gas at forebay and tailwater of dams reservoirs. In: Intelligent Data Analytics for Decision-Support Systems in Hazard Mitigation. Springer, Singapore, pp. 109–126, https://doi.org/10.1007/978-981-15-5772-9_6.

Heddam, S., Watts, M.J., Houichi, L., Djemili, L., Sebbar, A., 2018. Evolving connectionist systems (ECoSs): a new approach for modeling daily reference evapotranspiration (ET_0). Environ. Monit. Assess. 190 (9), 516. https://doi.org/10.1007/s10661-018-6903-0.

Hornik, K., 1991. Approximation capabilities of multilayer feedforward networks. Neural Netw. 4 (2), 251–257. https://doi.org/10.1016/0893-6080 (91)90009-T.

Hornik, K., Stinchcombe, M., White, H., 1989. Multilayer feedforward networks are universal approximators. Neural Netw. 2, 359–366. https://doi.org/10.1016/0893-6080 (89)90020-8.

Hrnjica, B., Mehr, A.D., Behrem, Š., Ağıralioğlu, N., 2019. Genetic programming for turbidity prediction: hourly and monthly scenarios. Pamukkale Üniversitesi Mühendislik Bilimleri Dergisi 25 (8), 992–997. https://doi.org/10.5505/pajes.2019.59458.

Huang, G.B., Chen, L., Siew, C.K., 2006a. Universal approximation using incremental constructive feedforward networks with random hidden nodes. IEEE Trans. Neural Netw. 17 (4), 879–892. https://doi.org/10.1109/TNN.2006.875977.

Huang, G.B., Zhu, Q.Y., Siew, C.K., 2006b. Extreme learning machine: theory and applications. Neurocomputing 70 (1–3), 489–501. https://doi.org/10.1016/j.neucom.2005.12.126.

Iglesias, C., Torres, J.M., Nieto, P.G., Fernández, J.A., Muñiz, C.D., Piñeiro, J.I., Taboada, J., 2014. Turbidity prediction in a river basin by using artificial neural networks: a case study in northern Spain. Water Resour. Manage. 28 (2), 319–331. https://doi.org/10.1007/s11269-013-0487-9.

Jaddi, N.S., Abdullah, S., Hamdan, A.R., 2015. Multi-population cooperative bat algorithm-based optimization of artificial neural network model. Inf. Sci. 294, 628–644. https://doi.org/10.1016/j.ins.2014.08.050.

Kasabov, N.K., Song, Q., 2002. DENFIS: dynamic evolving neural-fuzzy inference system and its application for time-series prediction. IEEE Trans. Fuzzy Syst. 10 (2), 144–154. https://doi.org/10.1109/91.995117.

Kasabov, N., Song, Q., Ma, T.M., 2008. Fuzzy-neuro systems for local and personalized modelling. In: Forging New Frontiers: Fuzzy Pioneers II. Springer, Berlin, Heidelberg, Germany, pp. 175–197.

Kisi, O., Heddam, S., Yaseen, Z.M., 2019a. The implementation of univariable scheme-based air temperature for solar radiation prediction: new development of dynamic evolving neural-fuzzy inference system model. Appl. Energy 241, 184–195. https://doi.org/10.1016/j.apenergy.2019.03.089.

Kisi, O., Khosravinia, P., Nikpour, M.R., Sanikhani, H., 2019b. Hydrodynamics of river-channel confluence: toward modeling separation zone using GEP, MARS, M5 Tree and DENFIS techniques. Stoch. Environ. Res. Risk Assess., 1–19. https://doi.org/10.1007/s00477-019-01684-0.

Liu, L.W., Wang, Y.M., 2019. Modelling reservoir turbidity using Landsat 8 satellite imagery by gene expression programming. Water 11 (7), 1479. https://doi.org/10.3390/w11071479.

Liu, Z., Jin, W., Mu, Y., 2020a. Variances-constrained weighted extreme learning machine for imbalanced classification. Neurocomputing. https://doi.org/10.1016/j.neucom.2020.04.052.

Liu, Q., Li, J., Wu, L., Wang, F., Xiao, W., 2020b. A novel bat algorithm with double mutation operators and its application to low-velocity impact localization problem. Eng. Appl. Artif. Intell. 90, 103505. https://doi.org/10.1016/j.engappai.2020.103505.

Luu, Q.H., Lau, M.F., Ng, S.P., Chen, T.Y., 2021. Testing multiple linear regression systems with metamorphic testing. J. Syst. Softw. 182, 111062. https://doi.org/10.1016/j.jss.2021.111062.

Mather, A.L., Johnson, R.L., 2014. Quantitative characterization of stream turbidity-discharge behavior using event loop shape modeling and power law parameter decorrelation. Water Resour. Res. 50 (10), 7766–7779. https://doi.org/10.1002/2014WR015417.

Mather, A.L., Johnson, R.L., 2016. Forecasting turbidity during streamflow events for two mid-Atlantic US streams. Water Resour. Manage. 30 (13), 4899–4912. https://doi.org/10.1007/s11269-016-1460-1.

Matouq, M., El-Hasan, T., Al-Bilbisi, H., Abdelhadi, M., Hindiyeh, M., Eslamian, S., Duheisat, S., 2013. The climate change implication on Jordan: a case study using GIS and Artificial Neural Networks for weather forecasting. J. Taibah Univ. Sci. 7 (2), 44–55. https://doi.org/10.1016/j.jtusci.2013.04.001.

Mehr, A.D., Nourani, V., 2018. Season algorithm-multigene genetic programming: a new approach for rainfall-runoff modelling. Water Resour. Manage. 32 (8), 2665–2679. https://doi.org/10.1007/s11269-018-1951-3.

Najah, A., El-Shafie, A., Karim, O.A., El-Shafie, A.H., 2013. Application of artificial neural networks for water quality prediction. Neural Comput. Applic. 22 (1), 187–201. https://doi.org/10.1007/s00521-012-0940-3.

Olyaie, E., Abyaneh, H.Z., Mehr, A.D., 2017. A comparative analysis among computational intelligence techniques for dissolved oxygen prediction in Delaware River. Geosci. Front. 8 (3), 517–527. https://doi.org/10.1016/j.gsf.2016.04.007.

Park, J.C., Um, M.J., Song, Y.I., Hwang, H.D., Kim, M.M., Park, D., 2017. Modeling of turbidity variation in two reservoirs connected by a water transfer tunnel in South Korea. Sustainability 9 (6), 993. https://doi.org/10.3390/su9060993.

Rajaee, T., Jafari, H., 2018. Utilization of WGEP and WDT models by wavelet denoising to predict water quality parameters in rivers. J. Hydrol. Eng. 23 (12), 04018054. https://doi.org/10.1061/(ASCE)HE.1943-5584.0001700.

Sebbar, A., Heddam, S., Kisi, O., Djemili, L., Houichi, L., 2020. Comparison of evolving connectionist systems (ECoS) and neural networks for modelling daily pan evaporation from Algerian dam reservoirs. In: Negm, A.M., Bouderbala, A., Chenchouni, H., Barceló, D. (Eds.), Water Resources in Algeria – Part I. The Handbook of Environmental Chemistry. vol. 97. Springer, Cham, Switzerland, https://doi.org/10.1007/698_2020_527.

Shekhar, C., Varshney, S., Kumar, A., 2020. Optimal control of a service system with emergency vacation using bat algorithm. J. Comput. Appl. Math. 364, 112332. https://doi.org/10.1016/j.cam.2019.06.048.

Škrjanc, I., Iglesias, J.A., Sanchis, A., Leite, D., Lughofer, E., Gomide, F., 2019. Evolving fuzzy and neuro-fuzzy approaches in clustering, regression, identification, and classification: a survey. Inf. Sci. 490, 344–368. https://doi.org/10.1016/j.ins.2019.03.060.

Teixeira, L.C., Mariani, P.P., Pedrollo, O.C., dos Reis Castro, N.M., Sari, V., 2020. Artificial neural network and fuzzy inference system models for forecasting suspended sediment and turbidity in basins at different scales. Water Resour. Manage. 34 (11), 3709–3723. https://doi.org/10.1007/s11269-020-02647-9.

Tsai, T.M., Yen, P.H., 2017. GMDH algorithms applied to turbidity forecasting. Appl. Water Sci. 7 (3), 1151–1160. https://doi.org/10.1007/s13201-016-0458-4.

Xie, X., Qin, X., Zhou, Q., Zhou, Y., Zhang, T., Janicki, R., Zhao, W., 2019. A novel test-cost-sensitive attribute reduction approach using the binary bat algorithm. Knowl.-Based Syst. 186, 104938. https://doi.org/10.1016/j.knosys.2019.104938.

Yang, X.S., 2010. A new metaheuristic Bat-inspired algorithm. In: González, J.R., Pelta, D.A., Cruz, C., Terrazas, G., Krasnogor, N. (Eds.), Nature Inspired Cooperative Strategies for Optimization (NICSO 2010). Studies in Computational Intelligence, vol. 284. Springer, Berlin, Heidelberg, Germany, https://doi.org/10.1007/978-3-642-12538-6_6.

Zhang, R., Wu, B., 2020. Environmental impacts of high water turbidity of the Niulan River to Dianchi Lake Water Diversion Project. J. Environ. Eng. 146 (1), 05019006. https://doi.org/10.1061/(ASCE)EE.1943-7870.0001623.

Zolfaghari, K., Wilkes, G., Bird, S., Ellis, D., Pintar, K.D.M., Gottschall, N., McNairn, H., Lapen, D.R., 2020. Chlorophyll-a, dissolved organic carbon, turbidity and other variables of ecological importance in river basins in southern Ontario and British Columbia, Canada. Environ. Monit. Assess. 192 (1), 1–16. https://doi.org/10.1007/s10661-019-7800-x.

Zounemat-Kermani, M., Alizamir, M., Fadaee, M., Sankaran Namboothiri, A., Shiri, J., 2020. Online sequential extreme learning machine in river water quality (turbidity) prediction: a comparative study on different data mining approaches. Water Environ. J. https://doi.org/10.1111/WEJ.12630.